Collective motion in nucleus-nucleus collisions at 800 MeV/nucleon

P. Danielewicz,[a] H. Ströbele,[b] G. Odyniec,[c] D. Bangert,[d] R. Bock,[b] R. Brockmann,[b] J. W. Harris,[c] H. G. Pugh,[c] W. Rauch,[e] R. E. Renfordt,[f] A. Sandoval,[b] D. Schall,[f] L. S. Schroeder,[c] and R. Stock [e]

[a]*Institute of Theoretical Physics, Warsaw University, 00-681 Warsaw, Poland*

[b]*Gesellschaft für Schwerionenforschung, D-6100 Darmstadt 11, Federal Republic of Germany*

[c]*Lawrence Berkeley Laboratory, University of California, Berkeley, California 94720*

[d]*Fachbereich Physik, Universität Marburg, D-3550 Marburg, Federal Republic of Germany*

[e]*Fachbereich Physik, Universität Frankfurt, D-6000 Frankfurt, Federal Republic of Germany*

[f]*Institut für Hochenergiephysik, Universität Heidelberg, D-6900 Heidelberg, Federal Republic of Germany*

(Received 23 November 1987)

Semicentral Ar+KCl, La+La, and Ar+Pb collisions at 800 MeV/nucleon were studied using a streamer chamber. The results are analyzed in the framework of the transverse momentum analysis and in terms of the average sphericity matrix. A critical examination of the analysis procedures, both experimental and theoretical, is given. New procedures are described to account for overall momentum conservation in the reaction, and to correct for azimuthal variations in the detection efficiency. Average transverse momenta per nucleon in the reaction plane are presented for deuterons emitted in the forward hemisphere, as these provide the most reliable information. A Vlasov-Uehling-Uhlenbeck calculation with a stiff equation of state gives a good fit to the momenta in the Ar+Pb reaction. Flow effects parametrized further using the sphericity tensor are found stronger than in the cascade model and consistently weaker than predicted by hydrodynamics. Parameters from the sphericity tensor exhibit a larger variation as a function of multiplicity than do the average momenta per nucleon.

I. INTRODUCTION

The collective flow of nuclear matter has recently been observed in high-energy nucleus-nucleus collisions,[1,2] in observations which have been made possible by the development of "4π" detectors such as the Streamer Chamber[3] and the Plastic Ball.[4,5] These detectors measure most of the charged particles emitted in the reaction. However, much work remains to be done to make a quantitative comparison between the extremely complex 4π data and the predictions of theoretical models such as hydrodynamics. To select the relevant features of the measurements, new methods of parametrizing the data have been devised, such as the sphericity (flow) analysis[6] and the transverse momentum analysis.[7] In addition to the difficulties intrinsic to such a comparison, there are practical problems, particularly in understanding the effect of detector acceptance limitations on the results. While 4π detectors are nearly complete in their angular coverage, they are not perfect in their ability to identify particles, measure momenta over the full dynamic range, etc.

In this paper we present measurements of the three reactions Ar + KCl, La + La, and Ar + Pb at 800 MeV/nucleon, obtained using the Streamer Chamber facility at the Bevalac. We describe the transverse-momentum-analysis method and introduce some new developments of it, testing each step by direct reference to the new data. We find that it is necessary to pay attention to overall momentum conservation, and provide a method for taking it into account. We also consider corrections for azimuthal variations in detection efficiency, and provide a method for making these corrections. The only other experimental problem is that of incomplete particle identification, which we discuss in detail. We conclude that the most reliable information on the average transverse momenta per nucleon in the reactions studied is provided by deuterons emitted in the forward hemisphere. We perform the transverse momentum analysis which leads also to the average sphericity tensor. Both the tensor parameters and the transverse momenta serve to display an A dependence and energy dependence of important collective flow effects.

II. EXPERIMENTAL PROCEDURE

The experimental procedure has been described previously.[3,8,9] In this section we present some details specific to the present measurements, a discussion of measurement losses, and a discussion of particle identification based on ionization measurements supplemented by kinematic considerations.

A. Streamer chamber exposure

The experiment was carried out at the Bevalac Streamer Chamber facility. The targets used were 0.60 g/cm^2 and 0.18 g/cm^2 KCl, 1.31 g/cm^2 Pb_3O_4, and 0.62 g/cm^2 La. The KCl and Pb_3O_4 targets were exposed to beams of ^{40}Ar, and the La target to a beam of ^{139}La, all at 800 MeV/nucleon. A plastic scintillator counter covering an angle around the beam axis of $\pm 8°$ in the laboratory,[10] with a signal proportional to ΣZ_i^2, has been used to select central events. In the Ar-KCl reaction this trigger was

adjusted to accept a fraction of 50% and 10% of the total inelastic cross section. The corresponding cross sections of 0.85 and 0.17 barn correspond in the geometrical picture to impact parameter cuts at 5.3 and 2.4 fm. The respective numbers for La + La and Ar + Pb reactions are 2.2 ($b < 8.5$ fm) and 1.0 barn ($b < 5.5$ fm). Reactions of Ar with oxygen in Pb_3O_4 were eliminated by the trigger.

B. Measurement of events on film

An unbiased sample of events in each reaction was selected for a semiexclusive measurement.[8,9] The Ar + KCl data were treated as one data sample consisting of 736 events from the more central trigger mode and 470 events from the more peripheral one. The momentum vectors for charged particles in the events were determined by reconstructing trajectories from the track images recorded on film in three views. Table I gives for each reaction the number of measured events together with characteristic features of the three data samples. The data for the Ar + KCl sample at 1.8 GeV/nucleon (previously referred to in Ref. 7 and again later in this paper) are also shown. The number of charged particles is deduced from the azimuthal distribution of the reconstructed tracks, assuming azimuthal symmetry around the beam axis.[8,9] This accounts for tracks lost at angles pointing towards and away from cameras. In the forward c.m. hemispheres of the reactions, the result is compatible with the anticipated value of $Z + N_{\pi^-}$, where Z is the projectile charge and N_{π^-} is the average number of π^- mesons per event. Note in Table I that the azimuthal losses increase with increasing multiplicity in the reactions. This is mainly due to the large number of flares and large streamer size caused by the high electric field required for sufficient streamer brightness in absence of image intensifiers. In the backward hemispheres, the numbers extrapolated from reconstructed particles show losses of up to 30% that are due to absorption in the target and steep streamer chamber tracks.

C. Particle identification

When data are to be subjected to Lorentz transformations, and/or relative particle abundances are to be studied, each track has to be associated with a definite particle. Particle identification in all three reactions is based on two different and independent methods.[8,9]

The first method relies on the correlation between the velocity of a charged particle and the energy loss in the streamer chamber gas exhibited in track brightness and streamer density. The quantification of the correlation in the data is hampered by the varying operation conditions of the streamer chamber, which lead to brightness variations even on the same picture. Taking the corresponding uncertainty into account, an ionization decision based on inspection of the track brightness and streamer distribution was restricted to tracks for which the different mass hypotheses led to a difference in ionization of more than 1. The track inclination with respect to the optical axis was accounted for. Furthermore, a value of the ionization of less than 5 times the minimum was demanded and the observed particles were assumed to be singly charged. For comparison, in the $^{93}Nb + {}^{93}Nb$ reaction at 650 MeV/nucleon, about 5% He contribution to the charged particle multiplicity is found.[11] The visual inspection of track density permits separation of π^+ from protons up to the laboratory momenta of 500 MeV/c. Protons are separated from deuterons in the momentum range of 800–1700 MeV/c. The latter separation, however, is not completely quantitative because of smaller differences in ionization[8] combined with problems from track superposition in high multiplicity events.

The second method of particle identification is based on kinematic considerations, together with the fact that in the interesting energy range the particle spectra from central collisions are fairly well described by a thermal fireball formed from participating baryons. For symmetric collisions at 800 MeV/nucleon, the kinematic particle identification (only for particles for which mass as-

TABLE I. Track statistics in the reactions at 0.8 GeV/nucleon and at 1.8 GeV/nucleon. (a) All tracks, (b) tracks in the forward c.m. system hemisphere.

Reaction	Ar + Pb		Ar + KCl		La + La		Ar + KCl
	(a)	(b)	(a)	(b)	(a)	(b)	(1.8 GeV/nucleon)
Number of events	956		1206		217		496
Number of tracks per event							
extrapolated (see text)	58.0	25.7	31.0	18.3	103.0	59.0	42.3
seen	49.6		29.3		80.2		40.7
reconstructed	46.4		28.3		71.1		38.0
Percentage of rejected tracks							
due to measuring errors	2.0%	1.1%					1.5%
due to $\Delta p_{lab} > p_{lab}/3$	2.0%	1.9%					0.2%
due to a bad vertex	1.8%	1.6%					2.0%
due to other reasons	3.2%	1.5%					2.7%
Number of π^- per event	2.4		1.3		4.0		4.6
Expected number of tracks in the forward c.m. system hemisphere				19.3		61	

signment from ionization was not possible) proceeds in several steps: (i) laboratory momenta of the baryons are Lorentz transformed into the c.m. system, assuming that the baryons are protons; (ii) a cut in the c.m. momentum set at 780 MeV/c selects those particles that are likely not to be protons; (iii) the laboratory momenta of those particles are now transformed again into the c.m. system, assuming the deuteron mass. A similar procedure with a cut in the c.m. momentum set at 1560 MeV/c separates the particles that are considered tritons. The kinematic cuts lead to proton-deuteron separation for laboratory momenta above 1700 MeV/c in the very forward direction and above 1100 MeV/c at a laboratory angle of 45°, with a certain overlap with the range of separation according to ionization. Figure 1 displays the proton and deuteron c.m. spectra in the c.m. angular range of 66°–90°, for the Ar + KCl reaction. The smoothness of the deuteron spectrum indicates the consistency of the identification procedure, as otherwise the cut in proton c.m. momenta at 780 MeV/c should yield a discontinuity in the deuteron spectrum at around 100 MeV deuteron kinetic energy. Figure 2 displays the spectra for the La + La reaction. Here a discontinuity around 100 MeV is visible, due to reduced efficiency of particle separation by ionization measurement in pictures with high track density. The situation for interactions of Ar with Pb is more complicated because the c.m. system is not *a priori* well defined as in symmetric systems. Therefore, a kinematical cut has been applied in this case at the laboratory momentum of 1750 MeV/c.

Figure 3 summarizes the deuteron identification in the symmetric reactions at 800 MeV/nucleon. The phase space of deuterons is projected onto the y-$p^{\perp}$ plane (y being determined in the laboratory frame assuming the deuteron mass). The shaded area represents the part of phase space in which the deuterons are identified. Specifically, in most of the forward hemisphere, and at large transverse momenta in the backward hemisphere, deuterons are identified by the kinematic cut procedure.

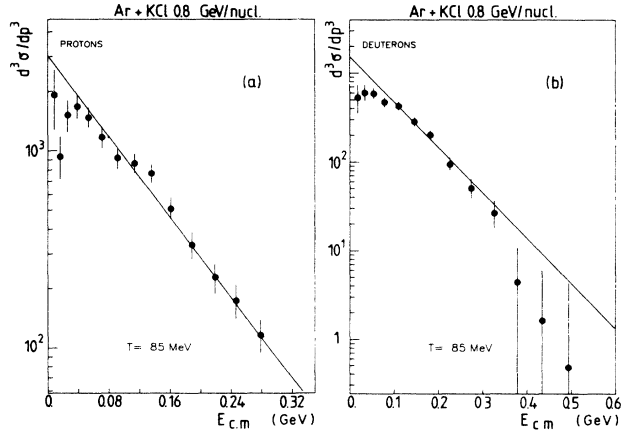

FIG. 1. Center-of-mass energy spectra (in arbitrary units) for (a) protons and (b) deuterons emitted between 66° and 90° c.m. angle for the Ar + KCl reaction at 0.8 GeV/nucleon. The straight line is for a Maxwell-Boltzmann distribution with a temperature of 85 MeV. The spectra are corrected for contaminations with d (a), t, and He particles.

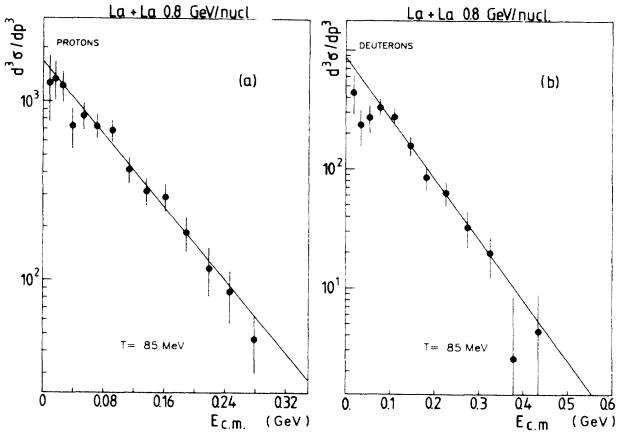

FIG. 2. Center-of-mass energy spectra (in arbitrary units) for (a) protons and (b) deuterons emitted between 66° and 90° c.m. angle for the La + La reaction at 0.8 GeV/nucleon. The straight line is for a Maxwell-Boltzmann distribution with a temperature of 85 MeV. The spectra are corrected for contaminations with d (a), t, and He particles.

In the remaining part of the forward hemisphere, and some of the backward hemisphere, deuterons are identified by the visual-inspection procedure. The remaining low $p^{\perp}$ part of the backward hemisphere is characterized by no or very limited d/p separation. An *a posteriori* illustration for the efficiency of the identification procedure is given in Fig. 4. The c.m. momentum distribution is presented in two angular domains: (a) $0.9 < \cos\theta^* < 1$ and (b) $0 < \cos\theta^* < 0.5$ for deuterons from ionization estimate and from the kinematical cuts. There are overlap regions around 500 MeV/c in (a) and 700 MeV/c in (b) in which the yield of the deuterons is very similar. Finally the deuteron, and also proton samples, contain a substantial triton and ^{3}He contribution. This has been corrected for in the spectra of Figs. 1 and 2; its influence on the transverse momentum analysis will be discussed in Sec. IV A.

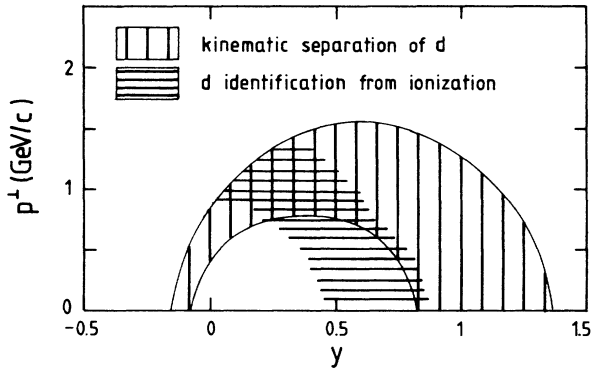

FIG. 3. The deuteron identification for symmetric reactions at 800 MeV/nucleon is illustrated by projecting the phase space of deuterons onto the y-$p^{\perp}$ plane (y being the laboratory rapidity); the vertically shaded area results from the kinematic cuts (see text) and the horizontally shaded area indicates the region of phase space where deuterons can be separated from protons on the basis of their ionization.

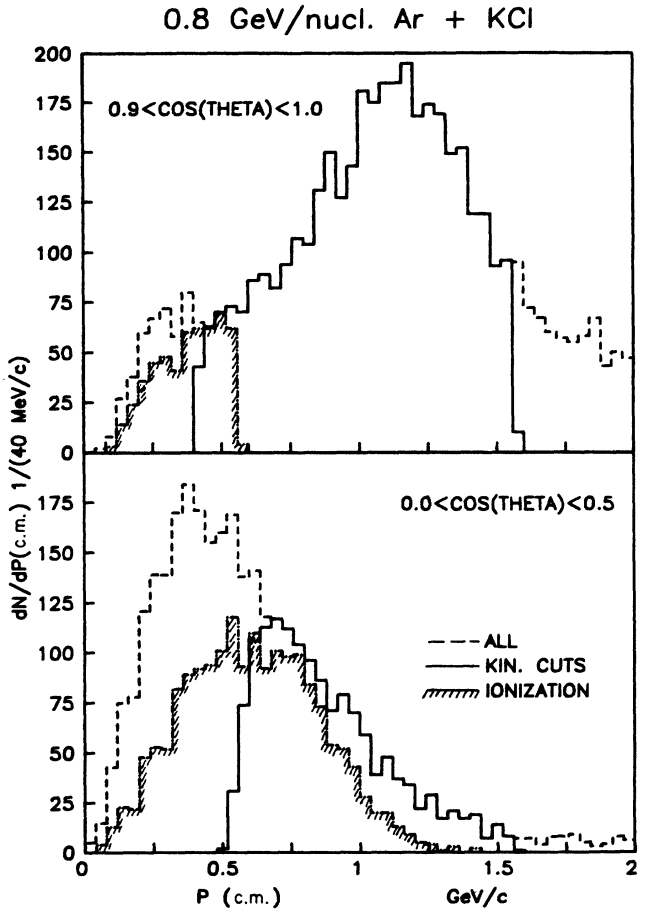

FIG. 4. Distribution of c.m. momenta of baryons (all treated as deuterons) in the reaction Ar + KCl at 0.8 GeV/nucleon in the angular range (a) $0.9<\cos\theta^*<1$ and (b) $0<\cos\theta^*<0.5$. Shown are all baryons (dashed line), deuterons identified by ionization (shaded histogram), and deuterons obtained by kinematical cuts. Note that if the kinematical cut selected particles as deuterons which previously had been identified as protons by their ionization the conflict was resolved in favor of the latter method.

III. THE TRANSVERSE MOMENTUM ANALYSIS

As stated in the Introduction we analyze collective motion in the reactions at 0.8 GeV/nucleon with the transverse momentum method. Since its initial formulation,[7] the method has been extensively used in data analysis.[12–20] Here we subject the method to a thorough scrutiny. A new form of data presentation is given. The method is extended with corrections for the overall transverse momentum conservation in collisions, and for the azimuthal inefficiencies of the experimental apparatus. Detailed discussions of the corrections are given in Appendices A and B. We show that the method may be used to evaluate parameters of an average sphericity matrix.

A. The basic concept

The method and data interpretation within the method rely on a symmetry of the colliding system: The nuclei approaching each other, in order to undergo a collision, obey a reflection symmetry with respect to the reaction plane defined for finite impact parameters by the beam axis and a line joining the centers of the nuclei. Though the structure of the colliding nuclei gets destroyed, the symmetry present in their initial state should be preserved throughout the course of a collision. The momentum distribution of nucleons in the nuclei is isotropic in transverse directions. With the spatial distribution of matter not having that property (for finite impact parameters), the momentum distribution should, in general, evolve from isotropy complying, however, with an overall reflection symmetry. The transverse momentum method attempts to exploit and quantify possible anisotropies in transverse momenta associated with the reaction plane. Because of the finite number of particles[21] a reflection symmetry with respect to the reaction plane may not be evident in every single final-state measurement. (One has to remark here that presumably for large deformations of initial nuclei, and sufficiently low impact parameters, such a symmetry cannot be claimed.) Nevertheless, for finite anisotropies any vector constructed from transverse particle momenta should, on the average, point in the direction of the reaction plane. In addition, the finite anisotropies and associated finite values of average in-plane momenta should render finite the average scalar product of transverse momenta and vectors constructed from the observed particles' momenta.

It was proposed in Ref. 7 to estimate the direction of the reaction plane for each event by means of a vector constructed from momenta $\mathbf{p}_\nu^\perp$ of observed particles:

$$\mathbf{Q}=\sum_\nu \omega_\nu \mathbf{p}_\nu^\perp , \tag{3.1}$$

with the weights ω_ν set to minimize the fluctuations of the vector around the direction of the plane. The weights $\omega_\nu=0$ were chosen for pions, while for the baryons $\omega_\nu=1$ for $y_\nu>y_c+\delta$, $\omega_\nu=-1$ for $y_\nu<y_c-\delta$, and $\omega_\nu=0$ otherwise. For a symmetric collision[7] it is natural to choose the rapidity y_c equal to the value of the overall c.m. system, $y_c=y_B/2$. The quantity δ was inserted to remove particles having negligible correlation with the reaction plane. The choice of weights followed from dynamic and symmetry considerations, and was verified *a posteriori*.

Particle transverse momenta are projected onto the direction determined from the vector $\mathbf{Q}$ to obtain[7,12–20] the mean components of transverse momenta in the *estimated* reaction plane for different rapidities. The magnitude of the vector $\mathbf{Q}$ can be used[7,15–17] to evaluate the mean components of momenta in the *true* reaction plane $\langle \omega p^x \rangle$, at rapidities $|y-y_c|>\delta$. The mean $\langle \omega p^x \rangle$ serves to rescale the components in the estimated reaction plane which are different from the components in the true reaction plane by a factor $\langle \cos\phi \rangle$. The angle ϕ is here the azimuthal deviation of the vector $\mathbf{Q}$ from the true reaction plane.

B. Factorization of scalar product average

The evaluation[7] of mean momenta in the true reaction plane $\langle \omega p^x \rangle$ is based on the presumption that the corre-

lation between particle transverse momenta is due to the anisotropies of momentum distributions associated with the reaction plane. For such a correlation the mean value of the scalar product of momenta of particles ν and μ at rapidities y_ν and y_μ should be

$$\langle \mathbf{p}_\nu^\perp(y_\nu)\cdot\mathbf{p}_\mu^\perp(y_\mu)\rangle \simeq \langle p_\nu^x(y_\nu)\rangle\langle p_\mu^x(y_\mu)\rangle \ , \tag{3.2}$$

with $\langle p_\nu^x(y_\nu)\rangle$ denoting mean in-plane transverse momentum of particle ν at rapidity y_ν. The possible validity of Eq. (3.2) has to depend on the magnitude of anisotropies associated with the reaction plane, as correlations from other sources can take over in the scalar product average. We shall see, indeed, that for weak dynamic effects in lighter systems, it can be necessary to take into account the overall transverse momentum constraint. Still, the analysis of transverse momenta may be carried out in such a way as to make the effect of an appropriate correction term to (3.2) negligible.

Equation (3.2) makes a strong prediction with respect to the data, implying an approximate factorization of a scalar product average into two functions of rapidity. To test the validity of Eq. (3.2), we analyze the average scalar product of deuteron transverse momenta from the La + La reaction at 0.8 GeV/nucleon. A contour plot of the deuteron $\langle \mathbf{p}^\perp(y_1)\cdot\mathbf{p}^\perp(y_2)\rangle$ is displayed in Fig. 5. The data have been collected in rapidity intervals of $\Delta y = y_B/6$, symmetrically with respect to the center-of-mass rapidity $y_c = y_B/2 \simeq 0.6$, providing 28 significant data points for the figure. Corrections for the azimuthal inefficiencies of the apparatus have been applied (Appendix A). For the graphic display, the data points have been approximated with a smooth surface for which the contour lines have been drawn. The features of the average scalar product of transverse momenta are seen in Fig. 5. There is a positive correlation of transverse momenta when both deuterons belong to the same outward area close to the projectile or target rapidity. There is a negative correlation of the momenta when particles fall into opposite areas of rapidity. This observation agrees with the expected opposite values of the in-plane transverse momenta $\langle p^x(y)\rangle$ in the two areas of rapidity ($y > y_c$ and $y < y_c$). By definition, the plot in Fig. 5 is symmetric with respect to the diagonal running from the bottom left to the upper right corner. Because of the symmetry of the colliding nuclei, the plot should be, however, further symmetric with respect to the diagonal running from the upper left to the bottom right corner. The lack of that symmetry indicates the systematic biases. However, if identification cuts, losses, and particle misidentifications do not break the azimuthal symmetry around the beam axis, they should not affect the possible factorization in (3.2), but, eventually, they will affect the values of average in-plane momenta.

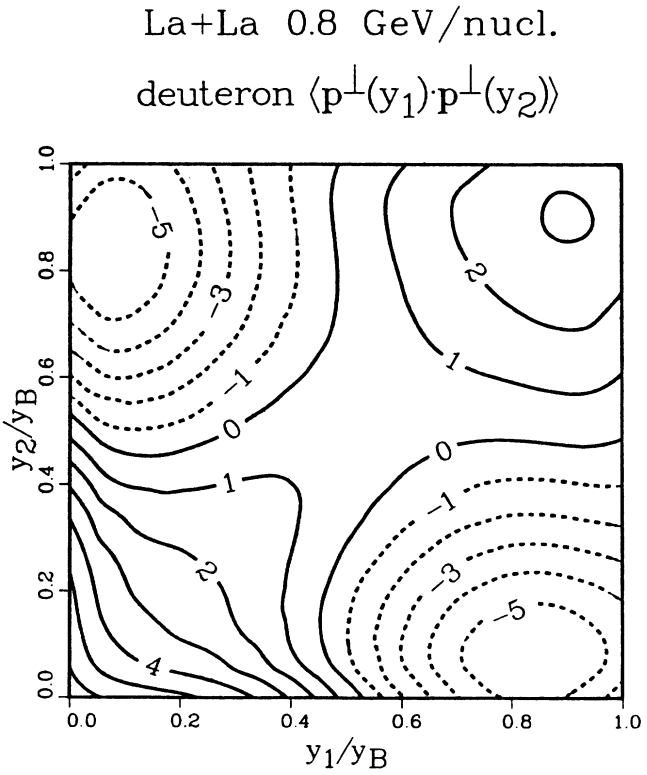

FIG. 5. Contour plot of the average scalar product of deuteron transverse momenta as a function of the corresponding two rapidities, for the La + La reaction at 0.8 GeV/nucleon. Contour lines are labeled with values of the product in units of 10^4 MeV$^2/c^2$.

C. The discretized scalar product matrix A_{ij}

Next, we turn to the statistical analysis of the average scalar product of deuteron momenta. The matrix $A_{ij} = \langle \mathbf{p}^\perp(y_i)\cdot\mathbf{p}^\perp(y_j)\rangle$, labeled with the discrete values of rapidity $y_i = (i-1)\Delta y$, is symmetric and may be diagonalized, $A_{ij} = \sum_k \lambda_k u_i^k u_j^k$ ($i,j,k = 1,\ldots,7$ in our case). Here u^k are eigenvectors normalized to unity. Equation (3.2) implies that, upon diagonalization, the matrix should be dominated by one positive eigenvalue λ_1 with an eigenvector $\lambda_1^{1/2} u^1(y_i) = \langle p^x(y_i)\rangle$. The eigenvalues for the matrix A_{ij} corresponding to the rapidity intervals are listed in Table II. There is, indeed, one dominant positive eigenvalue. Components of the associated eigenvector are shown in Fig. 6(a). For the fit to the matrix with the single most positive eigenvalue and associated eigenvector, $A_{ij} = \lambda_1 u_i^1 u_j^1$, we find $\chi^2 = 32$. (Any other

TABLE II. Eigenvalues from diagonalization of the average scalar product of deuteron transverse momenta discretized over rapidities, for the La + La and Ar + KCl reactions at 0.8 GeV/nucleon.

	λ_k (10^3 MeV$^2/c^2$)	
k	La + La	Ar + KCl
1	215±18	154±24
2	53±18	13±18
3	23±11	5±5
4	3±11	−4±5
5	−1±12	−9±9
6	−3±6	−18±20
7	−31±16	−67±12

single eigenvalue with a respective eigenvector yields $\chi^2 > 400.$) Still, for the given errors of matrix elements the diagonalization does not exactly correspond to the minimization of χ^2. The latter procedure, using Eq. (3.2), lowers χ^2 down to 25, and yields the seven values of $\langle p^x(y) \rangle$ shown in Fig. 6(c) (these constitute seven parameters for the 28 input data points), little changed from the values in Fig. 6(a).

Subsequently we consider the possible validity of Eq. (3.2) for the near symmetric reaction of the lighter nuclei Ar + KCl at 0.8 GeV/nucleon. A contour plot of $\langle \mathbf{p}^{\perp}(y_1) \cdot \mathbf{p}^{\perp}(y_2) \rangle$ for deuterons from the reaction is shown in Fig. 7. The data for the plot have been collected in the same manner as for the La + La reaction. Following Eq. (3.2) the scalar product average should be positive definite along the diagonal $y_2 = y_1$, while there are significant negative values on the diagonal in the figure. Table II lists the eigenvalues from the diagonalization of the matrix of average products of transverse momenta. A fit to the matrix with the largest positive eigenvalue and the associated eigenvector [see Fig. 8(a) for the components] yields $\chi^2 = 170$. The minimization of χ^2 using Eq. (3.2) lowers its value, but only down to 85. The failure of the fit is associated with the negative values of the average scalar product of momenta in the central area of Fig. 7. Indeed, the eigenvalues in Table II suggest that the matrix A_{ij} should be approximated by more than one term, i.e.,

$$A_{ij} \simeq \lambda_1 u_i^1 u_j^1 + \lambda_7 u_i^7 u_j^7 ,$$

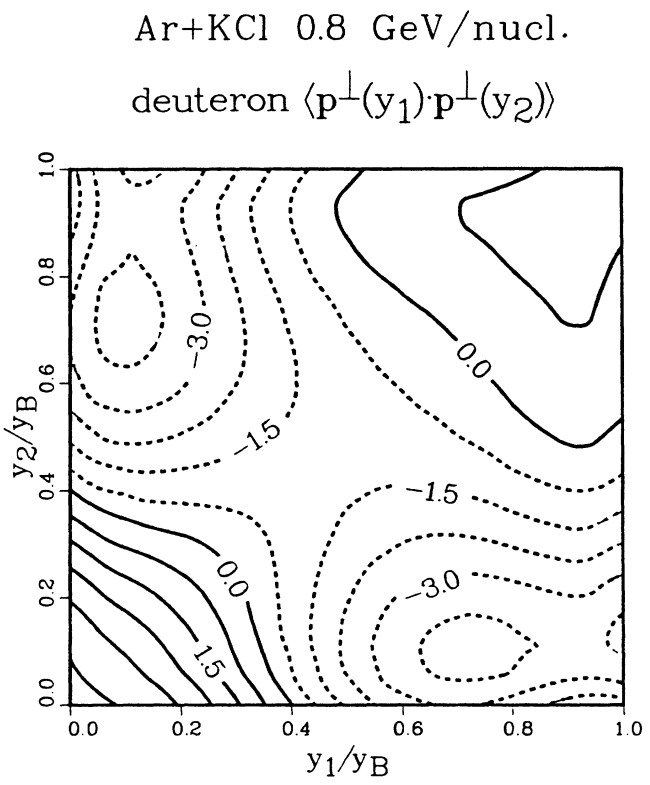

FIG. 7. Same as Fig. 4 for the Ar + KCl reaction at 0.8 GeV/nucleon.

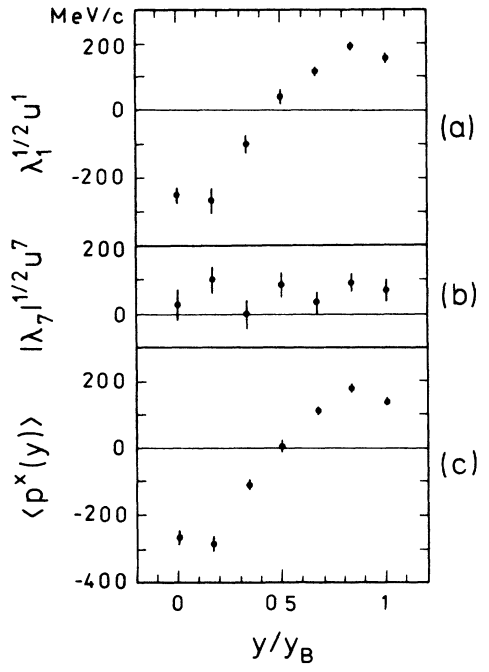

FIG. 6. Results from the analysis of $\langle \mathbf{p}^{\perp}(y_1) \cdot \mathbf{p}^{\perp}(y_2) \rangle$ for deuterons from the La + La reaction at 0.8 GeV/nucleon. (a) Components of an eigenvector associated with the largest positive eigenvalue. (b) Components of an eigenvector associated with the most negative eigenvalue. (c) Values of $\langle p^x(y) \rangle$ from the least squares fit.

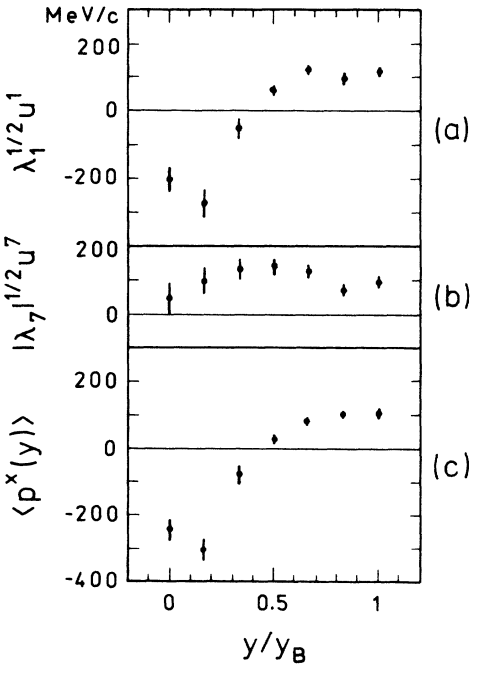

FIG. 8. Same as Fig. 5 for the Ar + KCl reaction at 0.8 GeV/nucleon.

where $\lambda_7 < 0$. Components of the eigenvector associated with the most negative eigenvalue are shown in Fig. 8(b).

D. Modification for momentum conservation

In order to explain this failure of the fit, we consider in Appendix B a general uncorrelated emission subject to total energy-momentum conservation, assuming a fixed direction of the reaction plane. We find that the transverse momentum conservation modifies Eq. (3.2) to

$$\langle \mathbf{p}_\nu^\perp(y_\nu)\cdot\mathbf{p}_\mu^\perp(y_\mu)\rangle \simeq \langle p_\nu^x(y_\nu)\rangle\langle p_\mu^x(y_\mu)\rangle - \alpha\langle p_\nu^{\perp 2}(y_\nu)\rangle\langle p_\mu^{\perp 2}(y_\mu)\rangle \ , \quad (3.3)$$

where α^{-1} is approximately equal to the sum of the particle transverse momenta squared in the final state of the system, $\alpha^{-1} \simeq \langle \Sigma_\mu p_\mu^{\perp 2}\rangle$. The correction term in (3.3) is of the order of $p^{\perp 2}/N$, where N is the number of particles in the final state. The term might be comparable with the first term in (3.3), for weak collective effects in the transverse momenta, $\langle p^x\rangle^2 \ll \langle p^{\perp 2}\rangle$. The origin of the correction term is essentially the following. As the transverse momentum $\mathbf{p}_\nu^\perp$ of a fragment ν fluctuates around the average $\langle \mathbf{p}_\nu^\perp\rangle = (\langle p_\nu^x\rangle, 0)$, the rest of the interacting system absorbs the recoil. For any given particle the share of the recoil is $\sim(\mathbf{p}_\nu^\perp - \langle \mathbf{p}_\nu^\perp\rangle)/N$, and a contribution from the recoil to the average scalar product of momenta of two fragments is then approximately

$$\langle p_\nu^\perp\cdot(p_\nu^\perp - \langle p_\nu^\perp\rangle)\rangle/N \simeq \langle p_\nu^{\perp 2}\rangle/N \ .$$

More properly, however, the result should be symmetric in the two fragments ν and μ, and this is accounted for in Eq. (3.3). Kinematic correlations between momenta from transverse momentum conservation had been observed in the high-energy hadron-hadron collisions[22,23] and used for estimating the number of missing neutrals in the final state of the reaction.

Using Eq. (3.3) we repeat the fit to the deuteron data from the Ar + KCl reaction, mapping out the values of the deuteron $\langle p^{\perp 2}(y)\rangle$, and treating α as a free parameter. We get now $\chi^2 = 18.0$, with values of $\langle p^x(y)\rangle$ unchanged within errors from those obtained using Eq. (3.2), and $\alpha^{-1} = 16.3 \pm 2.1$ $(\mathrm{GeV}/c)^2$. For comparison, with A denoting the total nucleon content of the colliding system, and $\langle p^{\perp 2}/a\rangle$ the average per-nucleon transverse momentum squared of identified nuclear fragments, we find in the Ar + KCl reaction $A\langle p^{\perp 2}/a\rangle \simeq 13$ $(\mathrm{GeV}/c)^2$.

In the case of the La + La reaction, Eq. (3.3) brings no improvement of the fit over Eq. (3.2), as χ^2 changes to 24. The momenta $\langle p^x(y)\rangle$ are unchanged within errors from those obtained using Eq. (3.2), and the deuteron data are consistent with large values of $\alpha^{-1} \gtrsim 74$ $(\mathrm{GeV}/c)^2$. For the La-La reaction we obtain $A\langle p^{\perp 2}/a\rangle \simeq 58$ $(\mathrm{GeV}/c)^2$.

To summarize the analysis up to this point, we do find that the deuteron data are explained by Eq. (3.2) for La + La, and by the extension (3.3) for Ar + KCl, which in turn assume an approximately uncorrelated particle emission in a coordinate system associated with the reaction plane.

E. Determination of average in-plane transverse momenta

In Eq. (3.3) an averaging may be introduced over rapidity and/or particle type for one or both particles in the product. This can be used for evaluating average in-plane transverse momenta and α in an alternative manner to the fit. With a weighting such as for the vector $\mathbf{Q}$, Eq. (3.1), in the equations deriving from (3.3),

$$\langle \mathbf{p}_\nu^\perp(y_\nu)\cdot\omega_\mu\mathbf{p}_\mu^\perp\rangle_{|y_\mu - y_c|>\delta} \simeq \langle p_\nu^x(y_\nu)\rangle\langle \omega p^x\rangle_{|y-y_c|>\delta} - \alpha\langle p_\nu^{\perp 2}(y_\nu)\rangle\langle \omega p^{\perp 2}\rangle_{|y-y_c|>\delta} \ , \quad (3.4)$$

$$\langle \omega_\nu\mathbf{p}_\nu^\perp\cdot\omega_\mu\mathbf{p}_\mu^\perp\rangle_{|y_{\nu,\mu}-y_c|>\delta} \simeq \langle \omega p^x\rangle_{|y-y_c|>\delta}^2 - \alpha\langle \omega p^{\perp 2}\rangle_{|y-y_c|>\delta}^2 \ , \quad (3.5)$$

the role of the recoil corrections can be reduced. If $\langle p^x(y)\rangle$ has different signs in the two areas of rapidity, $y > y_c + \delta$ and $y < y_c - \delta$, then the contributions to $\langle \omega p^x\rangle$ from the two areas are additive, and to $\langle \omega p^{\perp 2}\rangle$ subtractive. When particles occur with similar frequency in the two areas of rapidity, the value of $\langle \omega p^{\perp 2}\rangle$ can become negligibly small. In that case the use of Eqs. (3.4) and (3.5) to determine $\langle \omega p^x\rangle$ and $\langle p^x(y)\rangle$ is essentially equivalent to the procedure of Ref. 7. In general, however, the use of Eqs. (3.4) and (3.5) requires the knowledge of α the value of which can be determined arithmetically by solving the set of equations:

$$\begin{aligned}
&\langle \mathbf{p}_\nu^\perp\cdot\mathbf{p}_\mu^\perp\rangle_{y_{\nu,\mu}>y_c+\delta} \simeq \langle p^x\rangle_{y>y_c+\delta}^2 - \alpha\langle p^{\perp 2}\rangle_{y>y_c+\delta}^2 \ , \\
&\langle \mathbf{p}_\nu^\perp\cdot\mathbf{p}_\mu^\perp\rangle_{y_{\nu,\mu}<y_c-\delta} \simeq \langle p^x\rangle_{y<y_c-\delta}^2 - \alpha\langle p^{\perp 2}\rangle_{y<y_c-\delta}^2 \ , \\
&\langle \mathbf{p}_\nu^\perp\cdot\mathbf{p}_\mu^\perp\rangle_{\substack{y_\nu>y_c+\delta \\ y_\mu<y_c-\delta}} \simeq \langle p^x\rangle_{y>y_c+\delta}\langle p^x\rangle_{y<y_c-\delta} - \alpha\langle p^{\perp 2}\rangle_{y>y_c+\delta}\langle p^{\perp 2}\rangle_{y<y_c-\delta} \ .
\end{aligned} \quad (3.6)$$

F. Test of the procedure using cascade-model events

The procedure for determining average in-plane transverse momenta may be tested in the Cugnon[24] cascade model where the direction of the reaction plane is under control. In Table III the results following from Eqs. (3.5) and (3.6) are compared with the results obtained using the known direction of the reaction plane, for the following three reactions at 0.8 GeV/nucleon: Ar + KCl, La + La, and asymmetric Ar + Pb. Good agreement of the results is found. In the asymmetric Ar + Pb reaction, the rapidity y_c has been chosen smaller by 0.1 than the participant $y_{\mathrm{c.m.}}$ from protons[10,2] with $p^\perp > 270$ MeV/c. Table III contains further entries for parameters of the average per-nucleon sphericity matrix that can be found using the transverse momentum method.

G. Evaluation of the sphericity matrix

The average sphericity matrix associated with the reaction plane is defined as $\langle s^{ij}\rangle = \langle w p^i p^j/a\rangle$. Here w is a

weight taken usually as $1/2m$ or $1/p$, a is the mass number of a baryon, the momenta are in the c.m. system, and only baryons from the forward c.m. hemisphere, $y > y_{\text{c.m.}}$, are used for matrix evaluation. The difficult part in matrix evaluation is finding the element $\langle s^{xz} \rangle$ and resolving the transverse elements $\langle s^{xx} \rangle$ and $\langle s^{yy} \rangle$, as otherwise $\langle s^{zz} \rangle = \langle w p^{z2}/a \rangle$, $\langle s^{xx} \rangle + \langle s^{yy} \rangle = \langle w p^{\perp 2}/a \rangle$, and elements $\langle s^{yz} \rangle$ and $\langle s^{xy} \rangle$ vanish by reflection symmetry with respect to the reaction plane. Under the assumption of uncorrelated emission, the element $\langle s^{xz} \rangle$ may be obtained from an equation analogous to (3.4):

$$\langle w_\nu \mathbf{p}_\nu^\perp p_\nu^z \cdot \omega_\mu \mathbf{p}_\mu^\perp \rangle_{\substack{y_\nu > y_{\text{c.m.}} \\ |y_\mu - y_c| > \delta}} \simeq \langle s^{xz} \rangle \langle \omega p^x \rangle_{|y-y_c|>\delta} - \alpha \langle w p^{\perp 2} p^z \rangle_{y > y_{\text{c.m.}}} \langle \omega p^{\perp 2} \rangle_{|y-y_c|>\delta} . \tag{3.7}$$

The resolving of the elements $\langle s^{xx} \rangle$ and $\langle s^{yy} \rangle$ necessarily brings in a qualitatively new feature into the analysis. Specifically, one has to construct a two-dimensional tensor associated with the reaction plane with known average values of matrix elements, which is to be convoluted with the sphericity matrix. The tensor may be constructed using the momenta of two particles, and the following formula can be used for evaluating average elements of the sphericity matrix:

$$\langle w_\nu \omega_\mu \omega_\gamma \{ p_\nu^{\perp 2} (\mathbf{p}_\mu^\perp \cdot \mathbf{p}_\gamma^\perp) - 2 (\mathbf{p}_\nu^\perp \cdot \mathbf{p}_\mu^\perp)(\mathbf{p}_\nu^\perp \cdot \mathbf{p}_\gamma^\perp) \} \rangle_{\substack{y_\nu > y_{\text{c.m.}} \\ |y_{\mu,\gamma} - y_c| > \delta}} \simeq \{ \langle s^{yy} \rangle - \langle s^{xx} \rangle \} \langle \omega p^x \rangle^2_{|y-y_c|>\delta} . \tag{3.8}$$

The recoil corrections cancel out at the rhs of Eq. (3.8) to leading order. The use of Eq. (3.8) requires, unfortunately, considerably better statistics than, e.g., the use of Eq. (3.7).

When the sphericity matrix elements are known a diagonalization for the flow parameters[6] is straightforward. The eigenvalue that corresponds to an axis pointing out of the reaction plane is identical with $\langle s^{yy} \rangle$, $f_2 \equiv \langle s^{yy} \rangle$. The remaining eigenvalues and the flow angle θ_f are related to matrix elements with the equations

$$\begin{aligned} (f_3 - f_1) \sin 2\theta_f &= 2 \langle s^{xz} \rangle , \\ (f_3 - f_1) \cos 2\theta_f &= \langle s^{zz} \rangle - \langle s^{xx} \rangle . \end{aligned} \tag{3.9}$$

As can be seen in Table III, results for the flow parameters from the transverse momentum method are fairly consistent with those obtained with a known direction of the reaction plane.

TABLE III. Comparison of the results from the cascade model (Ref. 24) obtained using the known direction of the reaction plane (A) and using the transverse momentum method (B) for 1540 Ar + KCl events, 276 La + La events, and 1000 Ar + Pb events at 0.8 GeV/nucleon. The Ar + KCl events are combined from two samples for which impact parameter cuts are set according to the two trigger cross sections in the experiment, with event numbers, respectively, proportional to experimental event numbers for the two trigger modes. In calculating average momenta a value of $\delta = 0.15$ is used and in the asymmetric Ar + Pb reaction the rapidity y_c is taken smaller by 0.1 than the participant $y_{\text{c.m.}}$ (Refs. 10 and 2). The value of α^{-1} for the Cugnon cascade model should not be compared with an average sum of the final particle transverse momenta squared, but with a sum denoted in Table by $\mathcal{S}$, of the final *and* initial transverse momenta squared, excluding nucleons that have not undergone a collision. This is because the total initial transverse momentum in the model is *not* constrained to zero, but varies with the initial Fermi momenta of individual nucleons. Further, the nucleons that have not undergone a collision do not participate in the momentum exchange. For the sphericity matrix a weight $w = 1/p$ has been used. The eigenvalue ratios are $r_{ij} = f_i/f_j$ and $r = 2f_3/(f_1 + f_2)$.

	Ar + KCl 0.8 GeV/nucleon		La + La 0.8 GeV/nucleon $b < 8.5$ fm		Ar + Pb 0.8 GeV/nucleon $b < 5.5$ fm	
	(A)	(B)	(A)	(B)	(A)	(B)
$\langle \omega p^x \rangle_{\lvert y-y_c \rvert > \delta}$ (MeV/c)	32.2±1.7	33.2±3.6	65.2±2.2	64.7±2.6	43.3±1.5	40.0±2.2
$\langle p^x \rangle_{y > y_c + \delta}$ (MeV/c)	32.4±2.2	32±6	65.6±2.9	64.2±3.7	45.7±2.1	42±4
$\langle p^x \rangle_{y < y_c - \delta}$ (MeV/c)	−31.9±2.2	−34±7	−64.9±3.1	−66.7±3.7	−40.3±1.8	−37±4
$\mathcal{S}$ [(GeV/c)^2]	12.1±1.0		32.6±0.9		23.88±0.18	
α^{-1} [(GeV/c)^2]		13.5±0.8		33±6		27.2±2.8
θ_f (deg)	8.0±0.6	8.2±2.1	12.8±0.5	12.3±1.0	14.3±0.7	11.8±1.6
r_{31}	1.804±0.018	1.81±0.13	2.322±0.036	2.33±0.07	1.681±0.018	1.72±0.06
r_{32}	1.820±0.019	1.82±0.14	2.204±0.035	2.19±0.06	1.658±0.017	1.58±0.05
r_{21}	0.991±0.012	1.00±0.15	1.053±0.019	1.06±0.05	1.014±0.011	1.09±0.07
r	1.812±0.014	1.813±0.021	2.262±0.027	2.253±0.036	1.670±0.014	1.649±0.021

H. Correction of azimuthal detector efficiency variations

We complete this section with some discussion of corrections in data analysis for the azimuthal inefficiencies of the apparatus. The lack of uniformity in detection efficiency with respect to the azimuthal angle can generate a finite average of the scalar product of transverse momenta for particles emitted originally isotropically in the azimuthal angle. The main result of Appendix A is that weak nonuniformities may be remedied by correcting the transverse momenta entering into scalar products such as at the lhs of Eqs. (3.2)–(3.7). The amount of correction for each of the laboratory components of the transverse momentum is equal to the average value of that component for a given rapidity and fragment type. An illustration for the role of corrections in the determination of the reaction plane can be found in Ref. 9.

IV. RESULTS AND DISCUSSION

We are now ready to present results from the analysis of the data, selecting those parts which we find to be most reliable, and to compare them with theoretical expectations.

A. Average transverse momenta per nucleon

Average transverse momenta per nucleon in the reaction plane, resulting from Eq. (3.4), are shown in Fig. 9, for the three reactions at 0.8 GeV/nucleon: Ar + KCl, La + La, and Ar + Pb. The momenta are evaluated from deuterons only, for the following reason. As has been stated, the low-momentum deuterons belonging to the backward c.m. hemisphere cannot be differentiated in the streamer chamber from protons; when they are classified as protons, some fall in the backward and some in the forward hemisphere. As for a given rapidity the deuterons tend to have about twice as large transverse momenta in the reaction plane as protons, they bias the backward proton momenta towards high values, and the forward proton momenta towards low values. Specifically, one backward deuteron identified as a forward proton may neutralize the transverse momentum excess of two forward protons. The situation is more favorable for the deuteron sample. In the forward hemisphere all the protons are identified, and the ^{4}He particles have the same transformation characteristics as the deuterons because of the same charge to mass ratio. The triton and ^{3}He contribution to the deuterons is of the order of 35%. Extensive data simulations have shown, however, that the effect of the triton contribution on the deuteron sample is counterbalanced by the ^{3}He particles due to their different charge to mass ratios. The systematic errors on average deuteron transverse momenta from misidentification in the forward c.m. hemisphere turn out not to be larger than the statistical errors in this experiment.

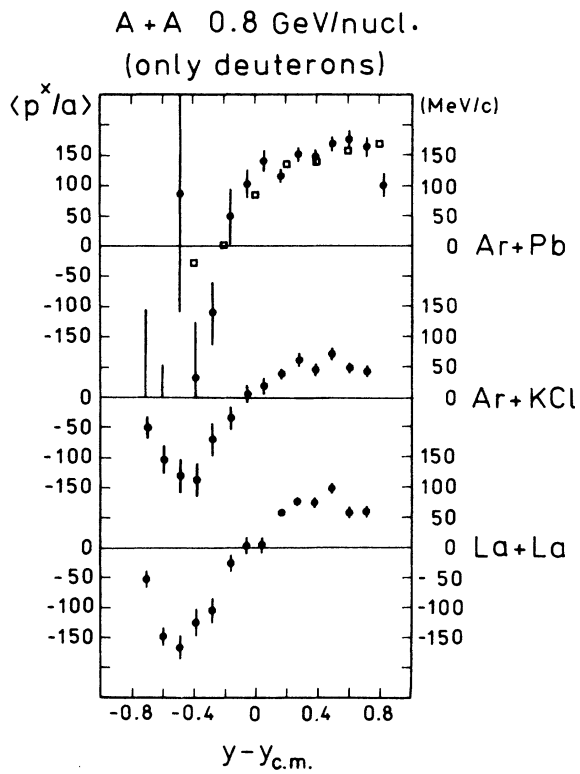

FIG. 9. Mean transverse momenta per nucleon in the reaction plane as a function of rapidity. Open squares for the Ar + Pb reaction indicate a prediction of the VUU calculation (Refs. 27 and 28).

High values of the average transverse momenta in the reaction plane in the backward c.m. hemisphere in Fig. 9, as compared with the forward hemisphere, are mostly due to the lack of identified deuterons with low $p^{\perp}$. (When a hole is cut out artificially in the forward hemisphere, analogous to the hole left by deuteron identification in the backward hemisphere (cf. Fig. 3) equally high average momenta in the reaction plane result in the forward as in the backward hemisphere.) Notably, a dependence of the average transverse momentum in the reaction plane, on the modulus of the transverse momentum vector, $\langle p^x(y,p^{\perp})\rangle$, deserves some future study.

It may be mentioned that while we quote the results for momenta from deuterons only, we use all baryons in the reference average $\langle \omega p^x \rangle_{|y-y_c|>\delta}$ in Eq. (3.4) to reduce statistical errors. When average in-plane transverse momenta of particles identified as protons are studied in the forward hemisphere, they are found lower by a factor of 2.5–3.5 from the full deuteron momenta. In the data and detection efficiency simulations this conforms with the supposition that the proton momenta are twice lower than the deuteron momenta for a given rapidity.

The average forward in-plane transverse momenta per nucleon are seen in Fig. 9 to increase with the mass of the colliding system, from about 50 MeV/c for the Ar + KCl system, through 70 MeV/c for La + La, up to about 140 MeV/c for Ar + Pb, cf. Table IV. The absence of geometric scaling[25] for the symmetric systems may be considered as a gradual onset of the hydrodynamic behavior with increasing mass of a system (see also Ref. 26). Indeed, if judged from the ratio of the trigger cross section to total inelastic cross section, the La + La events are even more peripheral than the Ar + KCl events. For the flow defined as a slope of $\langle p^x/a \rangle$, with respect to the

TABLE IV. Mean transverse momenta in the reaction plane in the forward rapidity region $y > y_c + \delta$. For the reactions at 0.8 GeV/nucleon, transverse momenta are evaluated from deuterons only and $\delta = 0.15$. For the Ar + KCl reaction at 1.8 GeV/nucleon $\delta = 0.3$ (cf. Ref. 7). Mean pion momenta evaluated with the same weighting as used for baryons are also given. The adopted multiplicity criteria approximately halve the samples of events for the reactions.

Reaction	Events	$\langle p^x/a \rangle_{y>y_c+\delta}$ (MeV/c/nucleon)	$\langle \omega p^x \rangle_{\pi^-}$ (MeV/c)	$\langle \omega p^x \rangle_{\pi^+}$ (MeV/c)	α^{-1} [(GeV/c)^2]
Ar + KCl	all	50±4	−4±7	4±6	16.3±1.2
0.8 GeV/nucleon	$M_p \leq 21$	44±4			11.8±1.5
	$M_p > 21$	56±6			18.5±1.7
La + La	all	72±6	0±5	7±9	110±40
0.8 GeV/nucleon	$M_p \leq 55$	78±8			75±50
	$M_p > 55$	66±8			130±70
Ar + Pb	all	139±7	4±5	11±6	38±6
0.8 GeV/nucleon	$M_p \leq 37$	122±6			45±17
	$M_p > 37$	156±11			35±8
Ar + KCl 1.8 GeV/nucleon	all	95±5	12±8	4±8	33±6

normalized rapidity,[19] we find ~100 MeV/c for the Ar + KCl reaction and ~140 MeV/c for the La + La reaction.

As to the variation with bombarding energy, we observe that the average momenta in the Ar + KCl reaction rise from 50 MeV/c at 0.8 GeV/nucleon, through 70 MeV/c at 1.2 GeV/nucleon,[15] up to 95 MeV/c at 1.8 GeV/nucleon.[7] At the last bombarding energy[7] the average momenta $\langle p^x/a \rangle$ were determined from all identified nuclear fragments, as the kinematic conditions for particle separation were more favorable, and the number of deuterons was lower than in the reaction at 0.8 GeV/nucleon.

In the asymmetric Ar + Pb reaction at 0.8 GeV/nucleon, it is seen in Fig. 9 that the results for $\langle p^x/a \rangle$ agree well with the predictions of the Vlasov-Uehling-Uhlenbeck (VUU) calculation[27,28] with a stiff equation of state. In the high-multiplicity ($M_p > 38$) events of the reaction, an interesting phenomenon occurs. The average number of nuclear charges in the rapidity area where $\langle p^x/a \rangle$ is positive (in the convention of Fig. 9) is of the order of 35. As this exceeds twofold the number of protons in the projectile, it is an indication that the part of the target hit by the projectile gets deflected to the side together with projectile fragments.

The momenta per nucleon $\langle p^x/a \rangle$ in the Ar + Pb reaction are the highest in absolute magnitude so far reported in the literature. Still, the momenta $\langle p^x/a \rangle$ are low compared with the rms transverse momenta per nucleon in the reaction, $\langle p^2/a \rangle^{1/2} \approx 520$ MeV/c in the forward hemisphere, or the longitudinal momenta. This is a rule in all the analyzed reactions[7,12–20] (but see the effects in the heavier composite particles in Ref. 29).

B. Sphericity matrix analysis

Some understanding of the phenomenon may be gained by considering a single-particle distribution associated with a reaction plane modeled with a Gaussian:[21]

$$\rho \propto \exp(-\tfrac{1}{2}\mathrm{Tr}\hat{s}\langle \hat{s} \rangle^{-1}) , \tag{4.1}$$

with

$$\langle \hat{s} \rangle = \hat{R}_y(\theta_{\mathrm{th}}) \hat{f}_{\mathrm{th}} \hat{R}_y(-\theta_{\mathrm{th}}) ,$$

where $\hat{f}_{\mathrm{th}} = \mathrm{diag}(f_1, f_2, f_3)$, $f_3 > f_1$, and $\hat{R}_y(\theta_{\mathrm{th}})$ is a rotation matrix about the y axis. The average transverse momentum in the reaction plane increases in the model linearly with the longitudinal momentum p^z:

$$\langle p^x(p^z) \rangle = p^z \frac{(f_3 - f_1)\sin\theta_{\mathrm{th}}\cos\theta_{\mathrm{th}}}{f_3\cos^2\theta_{\mathrm{th}} + f_1\sin^2\theta_{\mathrm{th}}} . \tag{4.2}$$

Physically, we expect large flow angles θ_{th} associated with shapes close to spherical, $f_3 - f_1 \ll f_3$. The momenta in the reaction plane are then suppressed by the factor $(f_3 - f_1)$ in Eq. (4.2). Clearly, no finite average momenta in the reaction plane can be expected for an ideally symmetric momentum distribution. On the other hand, we expect elongated shapes in association with small flow angles. (An exception here might be an emission of the heavier composite fragments, insensitive to a local spread of momenta.) Then the momenta are suppressed due to the factor $\sin\theta_{\mathrm{th}}$ in Eq. (4.2), as no finite values of the momenta can be expected for a shape directed exactly along the beam axis.

The above consideration indicates the usefulness of the knowledge of the sphericity matrix parameters for the reactions. The parameters are evaluated using formulas (3.7)–(3.9) from all baryons and are given in Table V. In the evaluation of the element $\langle s^{xz} \rangle$ and its error, the contamination of protons by deuterons is taken into account. (For a distribution of the flow angles on an event by event basis in the Ar + Pb reaction, see Ref. 2.) Comparing Table V with Table IV, it is seen that the sphericity matrix parameters vary more with multiplicity than do the average momenta $\langle p^x/a \rangle_{y>y_c+\delta}$. As parametrized by the tensor, the shapes associated with a reaction plane are generally prolate, with some preference for the momenta to be perpendicular to the reaction plane. Indeed, low flow angles are associated in the reactions with the elongated shapes, and larger flow angles with shapes

TABLE V. Parameters of the average per nucleon sphericity matrix with a weight $w=1/p$.

Reaction	Events	θ_f (deg)	r_{31}	r_{32}	r_{21}	r
Ar + KCl	all	9.6±0.8	2.96±0.10	2.68±0.07	1.11±0.06	2.81±0.04
0.8 GeV/nucleon	$M_p \leq 21$	7.2±0.6	4.36±0.20	3.75±0.14	1.16±0.09	4.03±0.06
	$M_p > 21$	13.7±1.2	2.17±0.09	2.00±0.07	1.09±0.08	2.08±0.04
La + La	all	16.5±1.7	2.24±0.10	2.09±0.05	1.07±0.05	2.16±0.06
0.8 GeV/nucleon	$M_p \leq 55$	14.5±1.7	2.69±0.14	2.51±0.08	1.07±0.07	2.60±0.08
	$M_p > 55$	19.3±1.7	1.94±0.08	1.80±0.06	1.08±0.06	1.87±0.06
Ar + Pb	all	35.6±1.8	1.96±0.26	1.52±0.07	1.28±0.12	1.71±0.14
0.8 GeV/nucleon	$M_p \leq 37$	28.8±1.2	2.24±0.13	1.85±0.06	1.21±0.07	2.03±0.07
	$M_p > 37$	42.4±1.4	1.8±0.3	1.34±0.10	1.36±0.18	1.55±0.18
Ar + KCl	all	8.5±1.0	3.20±0.11	3.16±0.11	1.01±0.06	3.18±0.05
1.8 GeV/nucleon						

closer to spherical symmetry. The relation between angle and elongation of the tensor $r=2f_3/(f_1+f_2)$ is further shown in Fig. 10. Tests with the data indicate that this relation is less sensitive to eventual cuts aimed at a spectator removal than are individual values for given multiplicities. The relation, cf. Fig. 10, shifts upward in angle with increasing mass of a system. Another quantity, that we actually refrain from evaluating here for reasons discussed at the beginning of the section, which can be expected to vary significantly with multiplicity, is the transverse momentum deposition discussed in Ref. 7.

C. Comparison with theory

First we compare the data with the predictions of the cascade model that we have already used in Sec. III. As can be seen from Table III and Fig. 10, the values of the flow angle from the Cugnon cascade model fall below the values inferred from the data for a given elongation of the tensor. With the exception of the La + La reaction, the

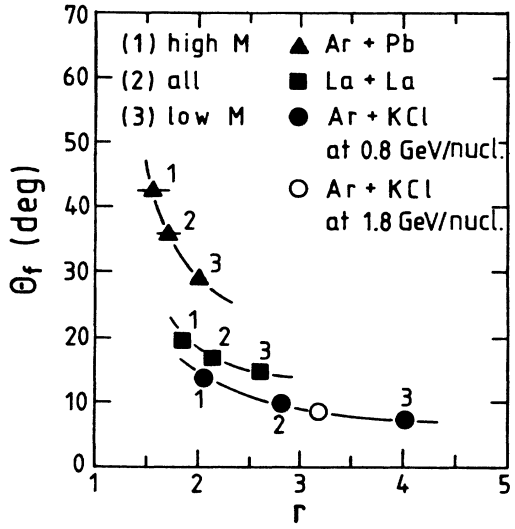

FIG. 10. Variation of the flow angle θ_f with elongation of the flow tensor $r=2f_3/(f_1+f_2)$.

average transverse momenta in the reaction plane are significantly lower in the cascade model than in the data (see Tables III and IV). For the studied symmetric reactions at 0.8 GeV/nucleon (Ar + KCl and La + La), the discrepancies, however, are not as large as for the Ar + Pb reaction or the Ar + KCl reaction[7] at 1.8 GeV/nucleon.

The measured transverse momenta and angles are both considerably lower than those from the ideal-fluid hydrodynamic model[30–33] at respective impact parameters or tensor elongations. (For a proper comparison, the results from the hydrodynamic model[30,31] for the symmetric reactions must be rescaled[25] according to the c.m. energy and size of the system.)

Macroscopically, what differentiates the cascade, Boltzmann-Uehling-Uhlenbeck[34,35] (BUU), or VUU,[36,37,27,28] and the hydrodynamic models, are the equation of state and the transport coefficients. A stiff equation of state enhances a collective motion.[36,37] On the other hand, an increase of the transport coefficients,[38,39] or equivalently a reduction of particle cross sections,[35,6] reduces the flow effects. In the Cugnon cascade model the equation of state should be close to that of an ideal gas, and the coefficients are sizable.[39] In the ideal-fluid calculations[30–32] the transport coefficients come in only from a numeric computation procedure. The equation of state is modified, in relation to that of an ideal gas, by adding a potential term depending on baryon density to the energy density. In first BUU and VUU calculations[34,36,37,27,28] the equation of state is constructed as in the hydrodynamic model, while transport coefficients are the same as in a cascade model.

Smaller than for other reactions, discrepancies between the cascade model results and the experimental results for the Ar + KCl and La + La reactions at 0.8 GeV/nucleon are presumably due to the fact that the equation of state in the model is stiff for the nuclear densities $\rho \lesssim 2\rho_0$. (The energy per baryon extrapolated to zero temperature is that of a degenerate ideal Fermi gas, without a minimum at $\rho=\rho_0$.)

The good agreement of the VUU model with experimental results from Ar + Pb at 0.8 GeV/nucleon, Ar + KCl at 1.8 GeV/nucleon[37] and 1.2

GeV/nucleon,[15,17] and Nb + Nb at 0.4 GeV/nucleon[27,14,19] reactions, shows that in that model a proper balance has been achieved between the stiffness of the equation of state and the magnitude of the transport coefficients. Still, it is not clear whether the equation of state and the coefficients could be changed simultaneously in such a way (see in that respect Ref. 35) that some agreement with these data is retained. If with the current parameters the VUU model underestimates the collective motion for lighter systems or large impact parameters at lower bombarding energies (such as the Ar + KCl and La + La reactions studied here), this could mean that transport coefficients need to be reduced and the equation of state softened. Not all of the pressure at high excitations, in addition, needs to be associated with a potential term in the energy density.

D. Summary

To summarize this paper we have presented new experimental results for the semicentral Ar + KCl, La + La, and Ar + Pb reactions at 0.8 GeV/nucleon, and analyzed them for collective motion using the transverse momentum method extended with corrections for azimuthal inefficiencies of the apparatus and transverse momentum conservation. The validity of the method has been tested using deuterons from the symmetric reactions. For all three reactions at 0.8 GeV/nucleon, we have obtained the average components of transverse momenta per nucleon in the reaction plane, as a function of the rapidity. These rise significantly with the mass of a colliding system reaching over 150 MeV/c/nucleon in the Ar + Pb reaction. From comparison with other data, a variation of the transverse momenta with bombarding energy has been observed in the Ar + KCl reaction. Furthermore, we have been able to evaluate parameters of an average sphericity matrix associated with the reaction plane for the reactions. The flow angle rises with the mass of a colliding system, and the flow parameters exhibit a larger variation with multiplicity than do the average momenta in the reaction plane.

ACKNOWLEDGMENTS

We wish to thank J. P. Branningan, the Bevalac staff, and the scanning and measuring group at the University of Heidelberg for their support. This work was supported in part by the U.S. Department of Energy under Contract No. DE-AC03-76SF00098, and by the Polish Ministry of Science and Higher Education Research Problem CPBP 01.09.

APPENDIX A

We discuss here the corrections for the nonuniformities in the azimuthal angle in the particle detection efficiency. The corrections may be applied in the data analysis when nonuniformities are weak.

We start with a consideration of the invariant distribution function of two fragments ν and μ, $\rho_{(2)}(\mathbf{p}_\nu^\perp, y_\nu, \mathbf{p}_\mu^\perp, y_\mu)$, assuming that the direction of the reaction plane is arbitrary from event to event, and that the distribution is normalized to unity with respect to integration over transverse momenta. We can put the distribution function into the form

$$\rho_{(2)}(\mathbf{p}_\nu^\perp, y_\nu, \mathbf{p}_\mu^\perp, y_\mu) = \rho(p_\nu^\perp, y_\nu)\rho(p_\mu^\perp, y_\mu) + \delta\rho_{(2)}(\mathbf{p}_\nu^\perp, y_\nu, \mathbf{p}_\mu^\perp, y_\mu) \ . \tag{A1}$$

Here ρ are the single-particle distributions (subject to an arbitrary direction of the reaction plane) and $\delta\rho_{(2)}$ is the correlation function responsible for the nonvanishing of an average scalar product of transverse momenta:

$$\int d\mathbf{p}_\nu^\perp d\mathbf{p}_\mu^\perp \mathbf{p}_\nu^\perp \cdot \mathbf{p}_\mu^\perp \delta\rho_{(2)}(\mathbf{p}_\nu^\perp, y_\nu, \mathbf{p}_\mu^\perp, y_\mu) = \langle \mathbf{p}_\nu^\perp(y_\nu) \cdot \mathbf{p}_\mu^\perp(y_\mu) \rangle \ . \tag{A2}$$

As demonstrated by the smallness of the scalar product averages compared with the average momenta squared (Secs. III and IV), $\delta\rho_{(2)}$ has to be considered a small correction to the product of single-particle distributions, $\delta\rho_{(2)} \ll \rho\rho$.

The apparatus modifies the two-particle distribution function with the factors of detection efficiency, $D(\mathbf{p}^\perp, y)$, which depend on components of the momenta in a coordinate system associated with the apparatus, making the observed distribution function equal

$$\rho_{(2)}^{\text{obs}}(\mathbf{p}_\nu^\perp, y_\nu, \mathbf{p}_\mu^\perp, y_\mu) = D(\mathbf{p}_\nu^\perp, y_\nu) D(\mathbf{p}_\mu^\perp, y_\mu) \rho_{(2)}(\mathbf{p}_\nu^\perp, y_\nu, \mathbf{p}_\mu^\perp, y_\mu) \ . \tag{A3}$$

The effect of D on averages from (A3) may be classified as twofold. The dependence of the efficiency on the modulus of the transverse momentum $p^\perp$, as, e.g., a high momentum cutoff, or a low momentum cutoff, for rapidities close to zero, changes an interpretation of the averages in such equations as (3.2)–(3.8). The averages are then not only restricted to a given rapidity or range of rapidities, but are also weighted in a certain manner with respect to the moduli of the momenta. (Such a feature is in practice common to any type of experimental analysis.) The dependence of D on the azimuthal angle, on the other hand, may simulate dynamic effects, by making an average scalar product of transverse momenta finite, in the absence of physical correlations between the directions of the momenta. The effects may be properly isolated when nonuniformities of the efficiency in the azimuthal angle are weak. We split D into

$$D(\mathbf{p}^\perp, y) = D_0(p^\perp, y) + D_1(\mathbf{p}^\perp, y) \ , \tag{A4}$$

where D_0 is equal to D averaged out over the azimuthal angle, and D_1 describes the nonuniformity in the angle. In that case, D_1 is related to an average momentum of a particle at given rapidity, as measured in a coordinate system associated with the apparatus, $\langle \mathbf{p}^\perp(y) \rangle^{\text{lab}}$, with

$$\frac{\int d\mathbf{p}^\perp \mathbf{p}^\perp D_1(\mathbf{p}^\perp, y)\rho(p^\perp, y)}{\int d\mathbf{p}^\perp D_0(p^\perp, y)\rho(p^\perp, y)} = \langle \mathbf{p}^\perp(y) \rangle^{\text{lab}} \ . \tag{A5}$$

When $|D_1| \ll D_0$ $[(\langle \mathbf{p}^\perp(y) \rangle^{\text{lab}})^2 \ll \langle p^{\perp 2} \rangle]$, the efficiency D_0 can be absorbed as a weighting function in

the *physical* averages, and to the second order in D_1 and first order in $\delta\rho_{(2)}$, the following equality holds:

$$\langle \mathbf{p}_\nu^\perp(y_\nu)\cdot\mathbf{p}_\mu^\perp(y_\mu)\rangle \simeq \langle \mathbf{p}_\nu^\perp(y_\nu)\cdot\mathbf{p}_\mu^\perp(y_\mu)\rangle^{\rm obs} - \langle \mathbf{p}_\nu^\perp(y_\nu)\rangle^{\rm lab}\cdot\langle \mathbf{p}_\mu^\perp(y_\mu)\rangle^{\rm lab} , \quad \text{(A6)}$$

where $\langle\cdot\rangle$ refers to the physical scalar product average, and $\langle\cdot\rangle^{\rm obs}$ to the measured average.

The correction for nonuniformity of the efficiency in the angle, the second term on the rhs of (A6), can be taken into account in the data analysis by mapping out the averages $\langle \mathbf{p}^\perp(y)\rangle^{\rm lab}$ for different fragments and then subtracting the product of the average laboratory momenta from the scalar product of the transverse momenta. Alternatively, the average laboratory momentum at a given rapidity may be subtracted from the momentum that enters into the scalar product, for one or both fragments in the product.

A similar consideration, adequate for the evaluation of the second moments of a distribution, Eq. (3.8), shows that there the nonuniformities in the azimuthal angle can be remedied to the leading order by subtracting average laboratory momenta from transverse momenta of *each* of the reference fragments, μ and ν.

APPENDIX B

We consider here a general uncorrelated emission in the coordinate system associated with the reaction plane, subject to the energy-momentum conservation constraint.

The assumption leading to Eq. (3.2) is that of an uncorrelated emission in the coordinate system associated with the reaction plane, taking for an invariant distribution function of two fragments ν and μ the form

$$\rho_{(2)}(\mathbf{p}_\nu^\perp,y_\nu,\mathbf{p}_\mu^\perp,y_\mu)=\rho(\mathbf{p}_\nu^\perp,y_\nu)\rho(\mathbf{p}_\mu^\perp,y_\mu) , \quad \text{(B1)}$$

with the product of single-particle distributions associated with the reaction plane on the rhs. On evaluating the average scalar product of transverse momenta at fixed fragment rapidities, one obtains, from (B1),

$$\begin{aligned}\langle \mathbf{p}_\nu^\perp(y_\nu)\cdot\mathbf{p}_\mu^\perp(y_\mu)\rangle &= \int d^2p_\nu^\perp d^2p_\mu^\perp \mathbf{p}_\nu^\perp\cdot\mathbf{p}_\mu^\perp\rho_{(2)}(\mathbf{p}_\nu^\perp,y_\nu,\mathbf{p}_\mu^\perp,y_\mu)/\int d^2p_\nu^\perp d^2p_\mu^\perp\rho_{(2)}\\ &= \left[\int d^2p_\nu^\perp \mathbf{p}_\nu^\perp\rho(\mathbf{p}_\nu^\perp,y_\nu)/\int d^2p_\nu^\perp\rho\right]\cdot\left[\int d^2p_\mu^\perp \mathbf{p}_\mu^\perp\rho(\mathbf{p}_\mu^\perp,y_\mu)/\int d^2p_\mu^\perp\rho\right]\\ &= \langle p_\nu^x(y_\nu)\rangle\cdot\langle p_\mu^x(y_\mu)\rangle , \end{aligned} \quad \text{(B2)}$$

with x denoting vector components in the reaction plane.

The assumption of uncorrelated emission ignores the energy-momentum constraint. Putting in the constraint implies a final-state exclusive distribution of particles of the form

$$\rho_{(N)}(\mathbf{p}_1^\perp,y_1,\ldots,\mathbf{p}_N^\perp,y_N)=\left[\prod_{\nu=1}^N\rho(\mathbf{p}_\nu^\perp,y_\nu)\right]\delta^{(4)}\left[\sum_{\nu=1}^N p_\nu - P\right] , \quad \text{(B3)}$$

with the four-momentum $P=(\mathbf{0},E)$ in the c.m. system. In (B3) it may be assumed that

$$\sum_{\nu=1}^N \langle p_\nu^\sigma\rangle = P^\sigma , \quad \text{(B4)}$$

where $\langle p_\nu^\sigma\rangle$ are the single-particle averages

$$\langle p^\sigma\rangle = \int d^2p^\perp dy\, p^\sigma\rho/\int d^2p^\perp dy\,\rho ,$$

and $\sigma=0,1,2,3$ designates the components of a four vector. This is because otherwise the single-particle distributions may be renormalized for (B4) with a factor $\exp(-\beta_\sigma\sum_\nu p_\nu^\sigma)$ on the rhs of (B3), and no alteration to the lhs of (B3). With the central-limit theorem one gets, from (B3) for the two-particle distribution,

$$\rho_{(2)}(\mathbf{p}_\nu^\perp,y_\nu,\mathbf{p}_\mu^\perp,y_\mu)\simeq\rho(\mathbf{p}_\nu^\perp,y_\nu)\rho(\mathbf{p}_\mu^\perp,y_\mu)\exp[-\tfrac{1}{2}A_{\sigma\tau}(p_\nu+p_\mu-\langle p_\nu\rangle-\langle p_\mu\rangle)^\sigma(p_\nu+p_\mu-\langle p_\nu\rangle-\langle p_\mu\rangle)^\tau] , \quad \text{(B5)}$$

where $A_{\sigma\tau}$ satisfies

$$A_{\sigma\tau}\sum_{\gamma\neq\nu,\mu}\langle(p_\gamma-\langle p_\gamma\rangle)^\tau(p_\gamma-\langle p_\gamma\rangle)^\kappa\rangle=\delta_\sigma^\kappa\ , \tag{B6}$$

and the sum runs over particles in the final state. The energy-momentum conservation constraint introduces an anticorrelation between the particle four-momenta. This is of the order of $1/N$. Of concern to us is the anticorrelation induced on the transverse particle momenta, and this might have been ignored, if not for the weakness of the collective effects (cf. Secs. III and IV) $\langle \omega p^x\rangle^2 \ll \langle p^{\perp 2}\rangle$:

$$\rho_{(2)}(\mathbf{p}_\nu^\perp,y_\nu,\mathbf{p}_\mu^\perp,y_\mu)\simeq\rho(\mathbf{p}_\nu^\perp,y_\nu)\rho(\mathbf{p}_\mu^\perp,y_\mu)\exp(-\alpha p_\nu^\perp\cdot p_\mu^\perp) \tag{B7}$$

with

$$\alpha^{-1}=\sum_{\gamma\neq\nu,\mu}\langle p_\gamma^{\perp 2}\rangle\approx\sum_\gamma\langle p_\gamma^{\perp 2}\rangle\ .$$

In (B7) we use the very weakness of the collective effects in transverse momenta. On expanding the exponential in (B6), we finally obtain Eq. (3.3). The similarity of the correction term for the momentum conservation to the basic result in the Goldhaber[40] model of statistical fragmentation should be noted (see also, Ref. 41).

[1]H. A. Gustafsson, H. H. Gutbrod, B. Kolb, H. Löhner, B. Ludewigt, A. M. Poskanzer, T. Renner, H. Riedesel, H. G. Ritter, A. Warwick, F. Weik, and H. Wieman, Phys. Rev. Lett. **52**, 1590 (1984).

[2]R. E. Renfordt, D. Schall, R. Bock, R. Brockmann, J. W. Harris, A. Sandoval, R. Stock, H. Ströbele, D. Bangert, W. Rauch, G. Odyniec, H. G. Pugh, and L. S. Schroeder, Phys. Rev. Lett. **53**, 763 (1984).

[3]A. Sandoval, R. Bock, R. Brockmann, A. Dacal, J. W. Harris, M. R. Maier, M. E. Ortiz, H. G. Pugh, W. Rauch, R. E. Renfordt, F. Riess, L. S. Schroeder, R. Stock, H. Ströbele, and K. L. Wolf, Nucl. Phys. **A400**, 365c (1983).

[4]A. Baden, H. H. Gutbrod, H. Löhner, M. R. Maier, A. M. Poskanzer, T. Renner, H. Riedesel, H. G. Ritter, H. Spieler, A. Warwick, F. Weik, and H. Wieman, Nucl. Instrum. Methods **203**, 189 (1982).

[5]H. H. Gutbrod, H. Löhner, A. M. Poskanzer, T. Renner, H. Riedesel, H. G. Ritter, A. Warwick, F. Weik, and H. Wieman, Nucl. Phys. **A400**, 343c (1983).

[6]M. Gyulassy, K. A. Frankel, and H. Stöcker, Phys. Lett. **110B**, 185 (1982).

[7]P. Danielewicz and G. Odyniec, Phys. Lett. **157B**, 146 (1985); Lawrence Berkeley Laboratory Report LBL-18600, 1984.

[8]H. Ströbele, Nucl. Instrum. Methods **221**, 523 (1984).

[9]H. Ströbele, Gesellschaftfür Schwerionenforschung Report GSI-86-10, 1986.

[10]H. Ströbele, R. Brockmann, J. W. Harris, F. Riess, A. Sandval, R. Stock, K. L. Wolf, H. G. Pugh, L. S. Schroeder, R. E. Renfordt, K. Tittel, and M. R. Maier, Phys. Rev. C **27**, 1349 (1983).

[11]K. G. R. Doss, H.-A. Gustafsson, H. H. Gutbrod, B. Kolb, H. Löhner, B. Ludewigt, A. M. Poskanzer, T. Renner, H. Riedesel, H. G. Ritter, A. Warwick, and H. Wieman, Phys. Rev. C **32**, 116 (1985).

[12]D. Keane, D. Beavis, S. Y. Fung, W. Gorn, Y. M. Liu, R. T. Poe, G. VanDalen, and M. Vient, in *Proceedings of the 2nd International Conference on Nucleus-Nucleus Collisions* (North-Holland Physics Publishing Division, Visby, 1985), Vol. 1, p. 3.

[13]J. P. Alard, J. Augerat, R. Babinet, N. Bastid, F. Brochard, N. De Marco, Z. Fodor, L. Fraysse, P. Gorodetzky, J. Gosset, D. L'Hôte, M. C. Mallet-Lemaire, G. Montarou, M. J. Parizet, J. Poitou, C. Racca, W. Schimmerling, J. C. Tamain, Y. Terrien, J. Valero, and O. Valette, see Ref. 12, Vol. 1, p. 6.

[14]H. G. Ritter, K. G. R. Doss, H. A. Gustafsson, H. H. Gutbrod, K. H. Kampert, B. Kolb, H. Löhner, B. Ludewigt, A. M. Poskanzer, A. Warwick, and H. Wieman, Nucl. Phys. **A447**, 3c (1985).

[15]D. Beavis, S. Y. Chu, S. Y. Fung, W. Gorn, D. Keane, Y. M. Liu, G. VanDalen, and M. Vient, Phys. Rev. C **33**, 1113 (1986).

[16]D. Keane, D. Beavis, S. Y. Chu, S. Y. Fung, W. Gorn, Y. M. Liu, G. VanDalen, and M. Vient, in Proceedings of the 4th Workshop on Nuclear Dynamics, Copper Mountain, Colorado, 1986 (unpublished).

[17]D. Keane, D. Beavis, S. Y. Chu, S. Y. Fung, W. Gorn, Y. M. Liu, G. VanDalen, M. Vient, J. J. Molitoris, and H. Stöcker, in Proceedings of the 2nd Conference on Intersections between Particle and Nuclear Physics, Lake Louise, Alberta, 1986 (unpublished).

[18]L. P. Csernai, P. Freier, J. Mevissen, H. Nguyen, and L. Waters, Phys. Rev. C **34**, 1270 (1986).

[19]K. G. R. Doss, H. A. Gustafsson, H. H. Gutbrod, K. H. Kampert, B. Kolb, H. Löhner, B. Ludewigt, A. M. Poskanzer, H. G. Ritter, H. R. Schmidt, and H. Wieman, Phys. Rev. Lett. **57**, 302 (1986).

[20]H. Białkowska, H. Agakishiev, I. Ivanovskaya, R. Mehtiev, V. Boldea, and S. Dita, Phys. Lett. B **173**, 349 (1986).

[21]P. Danielewicz and M. Gyulassy, Phys. Lett. **129B**, 283 (1983).

[22]J. H. Friedman, C. Risk, and D. B. Smith, Phys. Rev. Lett. **28**, 191 (1972).

[23]M. C. Foster, D. Z. Freedman, S. Nussinov, J. Hanlon, and R. S. Panvini, Phys. Rev. D **6**, 3135 (1972).

[24]J. Cugnon, Phys. Rev. C **22**, 1885 (1980).

[25]N. L. Balazs, B. Schürmann, K. Dietrich, and L. P. Csernai, Nucl. Phys. **A424**, 605 (1984).

[26]A. Bonasera and L. P. Csernai, Phys. Rev. Lett. **59**, 630 (1987).

[27]J. J. Molitoris, D. Hahn, and H. Stöcker, Nucl. Phys. **A447**, 13c (1985).

[28]J. J. Molitoris and H. Stöcker, Phys. Lett. **162B**, 47 (1985).

[29]J. W. Harris, B. V. Jacak, K.-H. Kampert, G. Claesson, K. G. R. Doss, R. Ferguson, A. I. Gavron, H.-A. Gustafsson, H. Gutbrod, B. Kolb, F. Lefebvres, A. M. Poskanzer, H.-G. Ritter, H. R. Schmidt, L. Teitelbaum, M. Tincknell, S. Weiss, H. Wieman, and J. Wilhelmy, Nucl. Phys. **A471**, 241c (1987).

[30]H. Stöcker, L. P. Csernai, G. Graebner, G. Buchwald, H. Kruse, R. Y. Cusson, J. A. Maruhn, and W. Greiner, Phys. Rev. C **25**, 1873 (1982).

[31]G. Buchwald, G. Graebner, J. Theis, J. Maruhn, W. Greiner,

H. Stöcker, K. Frankel, and M. Gyulassy, Phys. Rev. C **28**, 2349 (1983).
[32]L. P. Csernai, W. Greiner, H. Stöcker, I. Tanihata, S. Nagamiya, and J. Knoll, Phys. Rev. C **25**, 2482 (1982).
[33]H. Stöcker and W. Greiner, Phys. Rep. **137**, 277 (1986).
[34]G. F. Bertsch, H. Kruse, and S. Das Gupta, Phys. Rev. C **29**, 673 (1984).
[35]G. F. Bertsch, W. G. Lynch, and M. B. Tsang, Phys. Lett. B **189**, 384 (1987).
[36]H. Kruse, B. V. Jacak, and H. Stöcker, Phys. Rev. Lett. **54**, 289 (1985).
[37]J. J. Molitoris and H. Stöcker, Phys. Rev. C **32**, 346 (1985).
[38]J. Cugnon and D. L'Hôte, Nucl. Phys. **A452**, 738 (1986).
[39]P. Danielewicz, Phys. Lett. **146B**, 168 (1984).
[40]A. S. Goldhaber, Phys. Lett. **53B**, 306 (1974).
[41]B. K. Jennings, L. Satpathy, and S. Das Gupta, Phys. Rev. C **24**, 440 (1981).